2024 IEEE/RSJ International Conference on Intelligent Robots and Systems (IROS)
October 14-18, 2024. Abu Dhabi, UAE

A Robust and Efficient Robotic Packing Pipeline with Dissipativity-Based Adaptive Impedance-Force Control

Zhenning Zhou*, Lei Zhou*, Shengxin Sun, Marcelo H Ang Jr

***Abstract*—For humans, dense bin packing heavily relies on force perception. However, current robotic packing studies only focus on the visual input or adopt auxiliary push-to-place actions to eliminate gaps, suffering from high time expenditure and poor robustness. To address such limitations, we first introduce a novel external force estimation method based on the generalized momentum observer, which can avoid the influence of joint acceleration noises and achieve real-time high-precision monitoring. Second, to obtain compliant interaction and fine robustness, an adaptive variable impedance policy is developed to track dynamic motion and desired force, and compensate for uncertainties. Meanwhile, we perform dissipativity analysis and a virtual energy supply function is augmented to the system for optimization, providing a solid foundation for stability. Third, we propose an efficient packing methodology with three subtasks by considering the distinct interaction and constraint states in different areas. Our packing strategies eliminate the need for subsequent auxiliary actions and are proven to enhance efficiency. We perform quantitative evaluations to verify our external force estimation method, conduct comparison studies with current packing methods, and investigate the contribution of our dissipativity-based adaptive controller. The superior results not only prove the robustness and efficiency of our pipeline, but also pave the way for practical applications of packing.**

***Index Terms*—Bin packing, impedance-force control, dissipativity, momentum observer.**

I. Introduction

With the advantages of high automation and intelligence, robotic bin packing has attracted much interest in recent years [1] [2]. However, efficient and robust bin packing is still difficult because of the inaccuracies in vision and control. To the best of the authors' knowledge, there are few attempts to deploy bin packing solutions on real robots. The main challenge is to build efficient and robust packing policies while considering errors and uncertainties [3]. Meanwhile, the robot should properly react to the established interaction and avoid overshoots by adjusting the impedance parameters for compliance.

Extensive studies have been conducted on robotic bin packing. Robot systems for picking and packing specific items into the storage box have been proposed in the 2017 Amazon Robotics Challenge [4] [5]. Wang et al. [3] consider the packing task for irregular objects as a planning problem and present a constructive algorithm to search over the space of item positions and orientations. Similarly, the researchers [6] propose an offline bin packing algorithm by trying to maximize the utilization of free spaces in-between objects.

*Contribute equally. Zhenning Zhou, Shengxin Sun are from the Shanghai Jiao Tong University, Lei Zhou and Marcelo H Ang Jr are from the National University of Singapore. Corresponding author: Shengxin Sun (shengxin_sun700@sjtu.edu.cn). This research is supported by National Key R&D Program of China (Grant Number: 2018AAA0102700).

(a) Subtask-I: Packing objects in corners of the bin

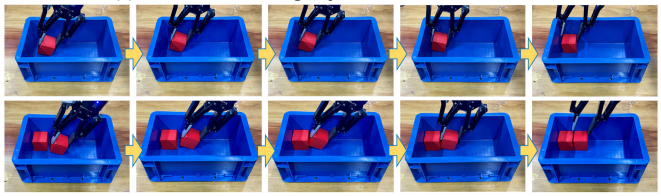

(b) Subtask-II: Packing middle objects under narrow spaces

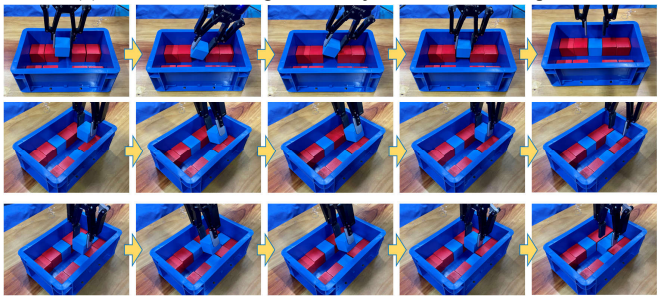

(c) Subtask-III: Inserting the last object

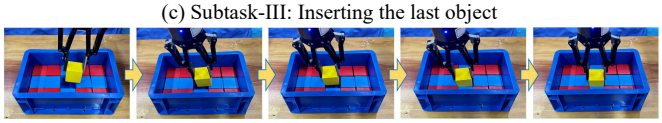

Fig. 1. The screenshots of dense packing for cuboid objects in each subtask. We divide the problem into three subtasks and design efficient packing strategies, which are deployed with the dissipativity-based adaptive controller.

By defining three key manipulation primitives, Shome et al. [7] propose a complete pipeline for cubic objects and take advantage of the environment and simple operations to achieve dense packing. Moreover, some aided means such as push actions [7] [8] [9] are studied to tightly place objects.

However, there remain some issues that limit the packing performance. First, most previous methods only adopt visual input to conduct packing while lacking external force perception, which leads to poor accuracy. Meanwhile, it is challenging to achieve high-precision real-time external force monitoring with joint torques due to the joint acceleration noise and the computational cost of the inversion of the robot inertia matrix. Second, the robot should properly react to the established contact and the control policy is desired to be adjusted adaptively during the dynamic interaction. However, these are always neglected by existing studies and result in poor robustness. Third, some research requires subsequent push-to-place actions after each object placement to correct errors and ensure compactness, which is effective but suffers from low efficiency. Dense and efficient packing policies that have no need for auxiliary actions remain to be explored.

To conquer these limitations, we first introduce an external force estimation method based on the generalized momentum observer, which can merely adopt the joint states of the robot to conduct real-time monitoring and achieve high accuracy. Then, based on the estimated external force, we further pro-

pose an adaptive impedance-force controller, which enables the robot to rapidly track desired motion and properly react to the established interaction. Meanwhile, the dissipativity analysis provides a solid foundation for system stability and conducts optimization with a virtual energy supply function. Moreover, we propose a dense packing methodology to divide this problem into three subtasks and design targeted strategies, as shown in Fig. 1, which improves the packing efficiency noticeably compared to conventional polices. Comprehensive experiments have been conducted and quantitative results prove that our proposed pipeline outperforms the existing methods by a large margin. Moreover, our pipeline is also tested on novel objects with different shapes and sizes, showing the generalizability of our pipeline for practical applications.

The contributions of our paper can be summarized as:

1) We introduce a novel external force estimation method, which is input with joint states and unaffected by acceleration noises, achieving high-accuracy monitoring.
2) An adaptive impedance-force controller is developed to achieve excellent performance in fine motion tracking and robust interaction using dissipativity analysis, which optimizes our controller to ensure system stability.
3) We propose an efficient packing methodology to divide the bin packing problem into three subtasks with designed strategies. Our method eliminates the need for subsequent auxiliary actions and significantly enhances efficiency.
4) The packing pipeline based on our controller and policies achieves the state-of-the-art performance in real-world robot experiments with improved efficiency and robustness.

II. Related Work

A. Bin Packing

Dense packing requires the objects to be placed in close vicinity to each other in an ordered manner [10]. Most current automatic packing deployments rely on using mechanical parts like conveyor trays [11], which are designed for specific products and difficult to modify or deploy. The robotic bin packing demands high levels of accuracy and robustness from the perception and the manipulation strategy. Some efforts have been conducted in the Amazon Robotics Challenge [4] [5] [12], but the problem that how to perform dense packing is not addressed in the proposed systems. Moreover, some researchers [13] [14] consider the NP-hard bin packing problem and focus on the problem of dense placement planning for a set of objects into a container. However, the perception and control strategies during packing are not discussed and there are few attempts to deploy bin packing solutions on real robots. Researchers [7] propose a pipeline for solving such packing tasks using RGB-D data and a robotic arm with a vacuum-based end effector. Nerveless, the subsequent push or pull actions are always desired after each placement for compactness, suffering from high time cost. Considering these, we propose an efficient and robust packing pipeline that contains adaptive control and manipulation policies for dense placement with vision and force perception.

B. Variable Impedance Control

The focus of variable impedance control is to adjust the impedance parameters adaptively based on the interaction with environments [15]. In recent years, many intelligent algorithms such as the fuzzy neural network [16] [17], reinforcement learning [18] [19] and learning control [20] have been adopted to adjust controller parameters. Pei et al. [21] propose to adjust the stiffness online based on the tracking error of the trajectory. Duan et al. [22] introduce a variable impedance controller to adapt environment stiffness uncertainties and track the dynamic desired force. Zhang et al. [23] recover the variable impedance policy from expert demonstrations with inverse reinforcement learning. These approaches can achieve fine motion and force tracking but there are always collisions during the contact, leading to force overshoot. For this problem, Cao et al. [24] [25] propose to adjust the impedance update rate and avoid the overshoot. However, these variable impedance control algorithms lack stability analysis from the mechanism perspective, leading to instability and inaccuracy during manipulation. Meanwhile, it is difficult to explain these unstable phenomena, and thus, researchers can only resort to empirical parameter tuning for optimization. We fill this gap with our dissipativity-based adaptive controller.

C. External Force Perception

External force perception is the basis of impedance control and compliant interaction with environments [26] [27]. Some researchers install the 6-axis force sensor between the robot TCP and the end effector to measure the external force. Ding et al. [28] adopt an OPTOFORCE F/T sensor to establish the transferable dynamics model. Liu et al. [29] employ an ATI Nano-43 sensor to provide force information for precision assembly. These installed F/T sensors are effective while increasing the cost of the robot system. For some collaborative robots, the joint sensors can measure joint torques. However, it is challenging to accurately estimate external force due to the influence of joint acceleration noise. Meanwhile, the computational cost of the inversion of the robot inertia matrix makes it difficult to ensure real-time measurement. To address the above problems, we propose a novel external force estimation method based on the generalized momentum observer, which avoids the inversion of the robot inertia matrix and eliminates the need for an estimate of joint accelerations.

III. External Force Estimation

We introduce a novel external force estimation method based on the generalized momentum observer for accurate monitoring. The dynamics for robots are described as follows:

$$\boldsymbol{M}(\boldsymbol{q})\ddot{\boldsymbol{q}} + \boldsymbol{C}(\boldsymbol{q},\dot{\boldsymbol{q}})\dot{\boldsymbol{q}} + \boldsymbol{g}(\boldsymbol{q}) = \boldsymbol{\tau} + \boldsymbol{\tau}_{ext} \tag{1}$$

where $\boldsymbol{\tau}$ and $\boldsymbol{\tau}_{ext}$ represent the joint and external torque, respectively. $\boldsymbol{q}$ denotes the actual joint position, $\boldsymbol{M}(\boldsymbol{q})$ is the mass matrix, $\boldsymbol{C}(\boldsymbol{q},\dot{\boldsymbol{q}})$ accounts for the centripetal and Coriolis torques, and $\boldsymbol{g}(\boldsymbol{q})$ corresponds to the gravitational torques.

The generalized momentum $\boldsymbol{p}$ of the robot is defined as:

$$\boldsymbol{p} = \boldsymbol{M}(\boldsymbol{q})\dot{\boldsymbol{q}} \tag{2}$$

A basic property of the robot dynamics is the skew-symmetry of matrix $\dot{\boldsymbol{M}}(\boldsymbol{q}) - 2\boldsymbol{C}(\boldsymbol{q},\dot{\boldsymbol{q}})$, which means $\dot{\boldsymbol{M}}(q) = \boldsymbol{C}(\boldsymbol{q},\dot{\boldsymbol{q}}) + \boldsymbol{C}^T(\boldsymbol{q},\dot{\boldsymbol{q}})$. Thus, we can obtain:

$$\begin{aligned}\dot{\boldsymbol{p}} &= \dot{\boldsymbol{M}}(\boldsymbol{q})\dot{\boldsymbol{q}} + \boldsymbol{\tau} + \boldsymbol{\tau}_{ext} - \boldsymbol{C}(\boldsymbol{q},\dot{\boldsymbol{q}})\dot{\boldsymbol{q}} - \boldsymbol{g}(\boldsymbol{q}) \\ &= \boldsymbol{\tau} + \boldsymbol{\tau}_{ext} + \boldsymbol{C}^T(\boldsymbol{q},\dot{\boldsymbol{q}})\dot{\boldsymbol{q}} - \boldsymbol{g}(\boldsymbol{q})\end{aligned} \tag{3}$$

Based on the expression of the dynamics of $\boldsymbol{p}$ in (3), we define the generalized momentum observer as:

$$\dot{\hat{\boldsymbol{p}}} = \boldsymbol{\tau} + \boldsymbol{r} + \hat{\boldsymbol{C}}^T(\boldsymbol{q},\dot{\boldsymbol{q}})\dot{\boldsymbol{q}} - \hat{\boldsymbol{g}}(\boldsymbol{q}) \tag{4}$$

And the residual equation is defined as:

$$\dot{\boldsymbol{r}} = \boldsymbol{K}_o(\dot{\boldsymbol{p}} - \dot{\hat{\boldsymbol{p}}}) \tag{5}$$

where $\boldsymbol{K}_o$ is the positive gain diagonal matrix of the observer. The observer output $\boldsymbol{r}(t)$ follows from integrating the (5):

$$\begin{aligned}\boldsymbol{r} &= \boldsymbol{K}_o\left[\int_o^t \dot{\boldsymbol{p}}(s)ds - \int_o^t \hat{\dot{\boldsymbol{p}}}(s)ds\right] \\ &= \boldsymbol{K}_o[\boldsymbol{p}(t) - \boldsymbol{p}(0) - \\ &\quad \int_0^t\left(\boldsymbol{\tau} + \boldsymbol{r} + \hat{\boldsymbol{C}}^{\mathrm{T}}(\boldsymbol{q},\dot{\boldsymbol{q}})\dot{\boldsymbol{q}} - \hat{\boldsymbol{g}}(\boldsymbol{q})\right)ds\Big]\end{aligned} \tag{6}$$

where $\boldsymbol{p} = \hat{\boldsymbol{M}}(\boldsymbol{q})\dot{\boldsymbol{q}}$, $\boldsymbol{r}(0) = \boldsymbol{0}$. When the estimated system dynamics parameters $\hat{\boldsymbol{M}}(\boldsymbol{q})$, $\hat{\boldsymbol{C}}^{\mathrm{T}}(\boldsymbol{q},\dot{\boldsymbol{q}})$ and $\hat{\boldsymbol{g}}(\boldsymbol{q})$ are equal to the ground truths, the dynamic relationship between the external joint torque $\boldsymbol{\tau}_{ext}$ and $\boldsymbol{r}$ can be expressed as:

$$\begin{aligned}\dot{\boldsymbol{r}} &= \boldsymbol{K}_{\mathrm{o}}(\dot{\boldsymbol{p}} - \hat{\dot{\boldsymbol{p}}}) \\ &= \boldsymbol{K}_{\mathrm{o}}\left[\boldsymbol{\tau} + \boldsymbol{\tau}_{ext} + \boldsymbol{C}^T\dot{\boldsymbol{q}} - \boldsymbol{g}(\boldsymbol{q}) - (\boldsymbol{\tau} + \boldsymbol{r} + \hat{\boldsymbol{C}}^T\dot{\boldsymbol{q}} - \hat{\boldsymbol{g}}(\boldsymbol{q}))\right] \\ &= \boldsymbol{K}_{\mathrm{o}}(\boldsymbol{\tau}_{ext} - \boldsymbol{r})\end{aligned} \tag{7}$$

Equation (7) can be regarded as a first-order system with $\boldsymbol{r}$ as a variable and $\boldsymbol{\tau}_{ext}$ as an input. The transfer function is:

$$\frac{\boldsymbol{r}(s)}{\boldsymbol{\tau}_{ext}(s)} = \frac{\boldsymbol{K}_{\mathrm{o}}}{s + \boldsymbol{K}_{\mathrm{o}}} \tag{8}$$

When $\boldsymbol{K}_{\mathrm{o}}$ is set as large values, $\boldsymbol{r}$ converges to $\boldsymbol{\tau}_{ext}$ exponentially and $\boldsymbol{r} \approx \boldsymbol{\tau}_{ext}$. Therefore, the external torque $\boldsymbol{\tau}_{ext}$ can be estimated by calculating $\boldsymbol{r}$ in (6), which avoids using joint accelerations and the inversion of the robot inertia matrix. This feature makes the momentum observer a kind of virtual sensor for external torques acting along the robot structure.

IV. Dissipativity-based Adaptive Impedance-Force Control Design

To achieve fine robustness during packing, we propose the dissipativity-based adaptive controller. The control law consists of three components: one to follow the desired motion with impedance characteristics, one to establish the desired contact force for stable interaction, and finally one to optimize the controller design using dissipativity-based stability analysis. Therefore, the input torque can be described as:

$$\boldsymbol{\tau} = \boldsymbol{\tau}_{imp} + \boldsymbol{\tau}_{frc} + \boldsymbol{\tau}_{opt} \tag{9}$$

where $\boldsymbol{\tau}_{imp}$, $\boldsymbol{\tau}_{frc}$ and $\boldsymbol{\tau}_{opt}$ are the input torques related to the motion control, force control and dissipativity-based control optimization, respectively, defined as follows.

A. Variable Impedance Control

Consider the dynamics model in the Cartesian space:

$$\boldsymbol{M}(\boldsymbol{x})\ddot{\boldsymbol{x}} + \boldsymbol{C}(\boldsymbol{x},\dot{\boldsymbol{x}})\dot{\boldsymbol{x}} + \boldsymbol{G}(\boldsymbol{x}) = \boldsymbol{J}^{-T}\boldsymbol{\tau} + \boldsymbol{F}_{ext} \tag{10}$$

where $\ddot{\boldsymbol{x}}$, $\dot{\boldsymbol{x}}$ and $\boldsymbol{x}$ are Cartesian acceleration, velocity and position of the end effector, respectively; $\boldsymbol{J}$ is the Jacobian matrix; $\boldsymbol{\tau}$, $\boldsymbol{F}_{ext}$ represent the joint space motor torque input and the external force, respectively. With the impedance control law, the robot will behave as a mass-spring-damping system, which follows the dynamics equation:

$$\boldsymbol{M}_d(\ddot{\boldsymbol{x}} - \ddot{\boldsymbol{x}}_d) + \boldsymbol{B}_d(\dot{\boldsymbol{x}} - \dot{\boldsymbol{x}}_d) + \boldsymbol{K}_d(\boldsymbol{x} - \boldsymbol{x}_d) = \boldsymbol{F}_{ext} \tag{11}$$

where $\boldsymbol{M}_d$, $\boldsymbol{B}_d$, $\boldsymbol{K}_d$ are the desired mass, damping and stiffness matrices, $\boldsymbol{x}_d$ is the desired trajectory. Considering (10) and (11) with $\boldsymbol{M}_d = \boldsymbol{M}(\boldsymbol{x})$, the control law can be written as:

$$\begin{aligned}\boldsymbol{\tau}_{imp} &= \boldsymbol{J}^T(\boldsymbol{B}_d\dot{\tilde{\boldsymbol{x}}} + \boldsymbol{K}_d\tilde{\boldsymbol{x}} + \boldsymbol{M}(\boldsymbol{x})\ddot{\boldsymbol{x}}_d + \boldsymbol{C}(\boldsymbol{x},\dot{\boldsymbol{x}})\dot{\boldsymbol{x}} + \boldsymbol{G}(\boldsymbol{x})) \\ \tilde{\boldsymbol{x}} &= \boldsymbol{x}_d - \boldsymbol{x}\end{aligned} \tag{12}$$

where $\tilde{\boldsymbol{x}}$ and $\dot{\tilde{\boldsymbol{x}}}$ are the tracking error and velocity error.

To enhance the robustness of robots in dynamic environments, we propose adaptation laws for the stiffness and damping parameters. Considering the stiffness parameter, the following adaptation law is applied:

$$K_d^i = K_o^i\left(1 - \exp\left(-\left(\frac{x_d^i - x^i}{x_d^i}\right)^2\right)\right) + K_c^i \tag{13}$$

In such a way, the robot behavior is stiffer when starting the tracking task, while becoming softer as soon as the reference pose $\boldsymbol{x}_d$ is reached. K_o^i , K_c^i are design parameters guiding the adaptation of the stiffness.

Considering the damping parameter, the following adaptation law is applied for the damping ratio:

$$h_d^i = h_o^i\exp\left(-\left(\frac{x_d^i - x^i}{x_d^i}\right)^2\right) + h_c^i \tag{14}$$

The damping parameter can be further calculated by $B^i = 2h_d^i\sqrt{K_d^i M_d^i}$. This way, the controlled robot behavior is less damped when starting tracking (to achieve a faster closed loop bandwidth), while becoming more damped as soon as the reference pose is reached (to avoid force overshoots).

B. Force Control

In our packing task, the manipulator generally establishes a constant contact force ${}^{ee}f_d$ along the *z*-direction with environments for stable performance. Thus, considering ${}^{ee}f_{ext}$ as the external force along the *z*-direction, the force control law is:

$$\boldsymbol{\tau}_{frc} = \boldsymbol{J}_{ee}^T(\boldsymbol{q})\left[{}^{ee}\boldsymbol{R},\ \boldsymbol{0}_{3\times3}\right]^T\left[0, 0, \lambda_{frc}\,{}^{ee}f_{frc}\right]^T \tag{15}$$

$${}^{ee}f_{frc} = {}^{ee}f_d + k_p\,{}^{ee}\tilde{f}_{ext} + k_i\int {}^{ee}\tilde{f}_{ext}dt + k_d\dot{\tilde{f}}_{ext} \tag{16}$$

$${}^{ee}\tilde{f}_{ext} = {}^{ee}f_d - {}^{ee}f_{ext} \tag{17}$$

where $\lambda_{frc}\,{}^{ee}f_{frc}$ and ${}^{ee}\tilde{f}_{ext}$ are the controller output and force tracking error, k_p , k_d , k_i are PID gains. The variable λ_{frc} is to deactivate the force controller when the robot gets too far from the desired motion. The logic behind this adaptation is to prioritize the motion control because constant contact force is not conducive to fast motion tracking when the tracking error is too large. Thus, λ_{frc} is defined as:

$$\lambda_{frc} = \lambda_{frc}^o - m_{frc}\left(\frac{x_d^j - x^j}{x_d^j}\right)^2 \tag{18}$$

where $\lambda_{frc}^o > 0$ and $m_{frc} > 0$ (with $\lambda_{frc}^o > m_{frc}$) are parameters guiding the adaptation law of the force control.

C. Dissipativity-based Stability Analysis and Optimization

This section conducts dissipativity-based stability analysis for the control system and optimizes our adaptive impedance-force controller with a virtual energy supply function.

Definition 1 [30]: A system is dissipative with respect to an energy supply function $s(\boldsymbol{u}(t), \boldsymbol{y}(t))$ if there exists a storage function $V(\boldsymbol{x}(t))$: $\mathrm{R}^n \rightarrow \mathrm{R}$ such that $V(\boldsymbol{0}) = 0$, $V(\boldsymbol{x}) \geq 0$ for all x, and

$$V(\boldsymbol{x}(T)) - V(\boldsymbol{x}(0)) \leq \int_0^T s(\boldsymbol{u}(t), \boldsymbol{y}(t))dt \tag{19}$$

for each input $\boldsymbol{u}(t)$, output $\boldsymbol{y}(t)$, and T in the interval of existence of the solution $\boldsymbol{x}(t)$.

Theorem 1 [30]: A dissipative system described in *Definition 1* can achieve the Lyapunov stability, if its supply function $s(\boldsymbol{u}(t), \boldsymbol{y}(t))$ satisfies:

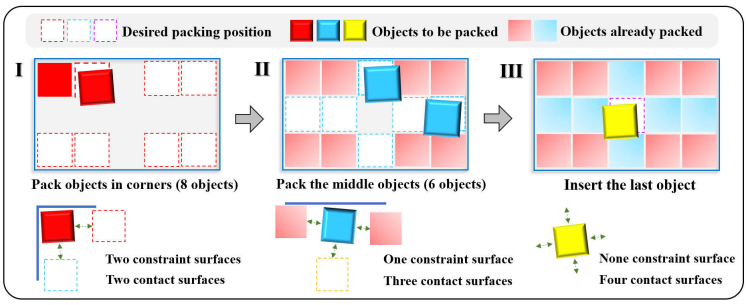

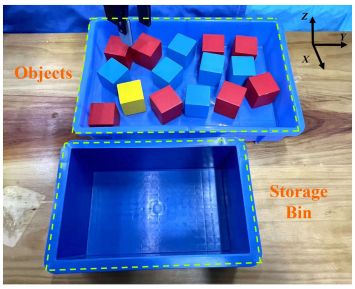

Fig. 2. (Left) Methodology for packing with different constraint and contact states. Reds represent the eight cubes in corners, blues denote the middle six cubes with already packed objects on both sides, and the yellow one is the last cube to be inserted. The constraint surfaces are the reliable conditions to maintain compactness, and the contact surfaces represent the directions of errors and contact with other objects. (Right) The initial configuration of the packing task.

$$s(\mathbf{0},\mathbf{0})=0,\ s(\mathbf{0},\boldsymbol{y})\le 0 \tag{20}$$

At first, to analyze the stability of the current control system ($\boldsymbol{\tau}=\boldsymbol{\tau}_{imp}+\boldsymbol{\tau}_{frc}$), we define the storage function as:

$$V(\dot{\tilde{\boldsymbol{x}}}(t),\tilde{\boldsymbol{x}}(t))=\frac{1}{2}\dot{\tilde{\boldsymbol{x}}}(t)^T\boldsymbol{M}(\boldsymbol{x})\dot{\tilde{\boldsymbol{x}}}(t)+\frac{1}{2}\tilde{\boldsymbol{x}}(t)^T\boldsymbol{K}_d(\boldsymbol{x})\tilde{\boldsymbol{x}}(t) \tag{21}$$

Rewrite (21) in differential form:

$$\frac{\partial V}{\partial t}=\dot{\tilde{\boldsymbol{x}}}^T\boldsymbol{M}(\boldsymbol{x})\ddot{\tilde{\boldsymbol{x}}}+\tilde{\boldsymbol{x}}^T\boldsymbol{K}_d\dot{\tilde{\boldsymbol{x}}}+\frac{1}{2}\dot{\tilde{\boldsymbol{x}}}^T\dot{\boldsymbol{M}}(\boldsymbol{x})\dot{\tilde{\boldsymbol{x}}}+\frac{1}{2}\tilde{\boldsymbol{x}}^T\dot{\boldsymbol{K}}_d\tilde{\boldsymbol{x}} \tag{22}$$

Considering (10), (12), and (15), we can obtain:

$$\frac{\partial V}{\partial t}=\frac{1}{2}\tilde{\boldsymbol{x}}^T\dot{\boldsymbol{K}}_d\tilde{\boldsymbol{x}}-\dot{\tilde{\boldsymbol{x}}}^T\boldsymbol{B}_d\dot{\tilde{\boldsymbol{x}}}-\dot{\tilde{\boldsymbol{x}}}^T(\boldsymbol{F}_{ext}+\boldsymbol{J}^{-T}\boldsymbol{\tau}_{frc}) \tag{23}$$

For this system, the output variable $\boldsymbol{y}(t)$ can be defined as $\boldsymbol{y}(t)=[\tilde{\boldsymbol{x}}^T(t),\dot{\tilde{\boldsymbol{x}}}^T(t)]^T$, and the input variable $\boldsymbol{u}(t)$ can be described as $\boldsymbol{u}(t)=\boldsymbol{F}_{ext}+\boldsymbol{J}^{-T}\boldsymbol{\tau}$. Thus, the energy supply function is given by $s(\boldsymbol{u},\boldsymbol{y})=\tilde{\boldsymbol{x}}^T\dot{\boldsymbol{K}}_d\tilde{\boldsymbol{x}}/2-\dot{\tilde{\boldsymbol{x}}}^T(\boldsymbol{F}_{ext}+\boldsymbol{J}^{-T}\boldsymbol{\tau}_{frc})$, and then the energy inequality (19) can be satisfied. However, based on *Theorem 1*, it is obvious that $s(\mathbf{0},\boldsymbol{y})=\tilde{\boldsymbol{x}}^T\dot{\boldsymbol{K}}_d\tilde{\boldsymbol{x}}/2$ cannot always guarantee the Lyapunov stability, which leads to the system potentially unstable.

To address this problem, we construct a dissipativity-based control optimization term (24) to obtain the controller in (9) with the proposed virtual energy supply function $s_v(\rho_v)$:

$$\boldsymbol{\tau}_{opt}=\frac{-\boldsymbol{J}^T\dot{\tilde{\boldsymbol{x}}}}{\|\dot{\tilde{\boldsymbol{x}}}\|^2}\cdot s_v(\rho_v) \tag{24}$$

$$s_v(\rho_v)=\frac{\partial}{\partial t}\left(\frac{1}{2}\rho_v(t)^T\rho_v(t)\right) \tag{25}$$

where $\rho_v(t)$ denotes the virtual dynamics as (26), and γ represents the dynamic parameter as (27).

$$\dot{\rho}_v(t)=-\frac{\gamma}{2\rho_v(t)}\tilde{\boldsymbol{x}}^T\dot{\boldsymbol{K}}_d\tilde{\boldsymbol{x}} \tag{26}$$

$$\gamma=\begin{cases}1, & \text{if } \frac{1}{2}\tilde{\boldsymbol{x}}^T\dot{\boldsymbol{K}}_d\tilde{\boldsymbol{x}}\ge 0\\ 0, & \text{otherwise}\end{cases} \tag{27}$$

In this case, the derivative of the new storage function V_w with our supplemented control term τ_{opt} can be derived as:

$$\frac{\partial V_w}{\partial t}=\frac{1-\gamma}{2}\tilde{\boldsymbol{x}}^T\dot{\boldsymbol{K}}_d\tilde{\boldsymbol{x}}-\dot{\tilde{\boldsymbol{x}}}^T\boldsymbol{B}_d\dot{\tilde{\boldsymbol{x}}}-\dot{\tilde{\boldsymbol{x}}}^T(\boldsymbol{F}_{ext}+\boldsymbol{J}^{-T}\boldsymbol{\tau}_{frc}) \tag{28}$$

Meanwhile, the whole energy supply function $s_w(\boldsymbol{u},\boldsymbol{y})$ with $s_v(\rho_v)$ is expressed as (29), which satisfies $s_w(\mathbf{0},\boldsymbol{y})\le 0$.

$$s_w(\boldsymbol{u},\boldsymbol{y})=\frac{1-\gamma}{2}\tilde{\boldsymbol{x}}^T\dot{\boldsymbol{K}}_d\tilde{\boldsymbol{x}}-\dot{\tilde{\boldsymbol{x}}}^T(\boldsymbol{F}_{ext}+\boldsymbol{J}^{-T}\boldsymbol{\tau}_{frc}) \tag{29}$$

Therefore, considering (28) and (29), the conditions in *Definition 1* and *Theorem 1* can be satisfied, and the whole system with our controller (9) is dissipativity-based stable.

V. Packing Methodology

In this section, we propose an efficient packing methodology that eliminates the need for subsequent push-to-place actions. By considering the distinct interaction and constraint states in different areas of the storage bin, we divide the packing task into three subtasks, which are packing the first objects in corners, packing the middle objects under narrow spaces, and inserting the last object, as shown in Fig. 2. Moreover, some visual algorithms are adopted for object grasping and guiding the robot to desired positions.

A. Grasping and Preliminary Packing

For each object, a pre-defined grasp library $(\boldsymbol{\phi}_i^g,\boldsymbol{\varphi}_i^g)$ is established in object-centric manner. Once object pose $\boldsymbol{\varphi}_i$ is obtained through the incorporated pose estimation algorithm AAE [31], the corresponding collision-free manipulator pose $\boldsymbol{\phi}_i$ in the base frame for motion planning can be calculated:

$$\boldsymbol{\phi}_i \longleftarrow \left\{is\_pick\_collisionless((\boldsymbol{\phi}_i^g,\boldsymbol{\varphi}_i^g),\boldsymbol{\varphi}_i)=True\right\} \tag{30}$$

Moreover, we establish prior knowledge $(\boldsymbol{\lambda}_j^p,\boldsymbol{\gamma}_j^p)$ between the bin pose and the poses of objects to be packed based on the packing order. In this case, the desired object pose $\boldsymbol{\gamma}_d^j$ for each preliminary placement in the base frame can be obtained by calculating the bin pose $\boldsymbol{\lambda}_j$ and the prior knowledge:

$$\boldsymbol{\gamma}_d^j \longleftarrow \{(\boldsymbol{\lambda}_1^p,\boldsymbol{\gamma}_1^p),...,(\boldsymbol{\lambda}_n^p,\boldsymbol{\gamma}_n^p),\boldsymbol{\lambda}_j\},\ j\in[1,n] \tag{31}$$

where n represents the total number of objects to be packed.

B. Subtask-I: Packing the Objects in Corners

Subtask-I aims to pack the first objects in four corners. However, there always exists a residual gap larger than the thickness of the finger ε due to the contact of the gripper and storage bin. Previous research adopts subsequent push actions but suffers from high time expenditure. To address this issue, we propose a packing strategy to achieve tight placement just in one step, as presented in Fig. 3. The angle α can be calculated based on the grasp depth d, the size of the object ℓ and the thickness of the gripper ε:

$$\alpha=\pi/2-\arctan(\varepsilon/(\ell-d)) \tag{32}$$

We summarize the proposed method in Algorithm 1. When the robot has been guided near the desired position, first, the manipulator tilts around the end and moves down along the z-direction. The constant force is simultaneously

held for stability. Then, the manipulator moves towards the x-direction of the storage bin until the object and bin are in tight contact, which denotes that the external force in this direction is greater than 5 N. Meanwhile, the rotation error can be eliminated with the external torque about the z-axis. Afterwards, the manipulator moves towards the y-direction, and when the object also constructs tight contact with the bin in this direction, the approach process is finished. Finally, the manipulator rotates to narrow the gap with an angle α, and the gripper opens to release the object. During the whole process, the desired motion trajectory and force are tracked by our adaptive impedance-force controller.

Algorithm 1: Strategy for packing objects in corners

Input: Six-dimension external force/torque $\boldsymbol{F}_{ext}$, $\boldsymbol{T}_{ext}$
Tilt around the end
In every force control cycle S_c*:*
  If $F_z > 0$ **then**
    Maintain constant force with bin in the z-direction
    If $F_x < F_{contact}$ **then**
      The end of the robot moves along the x-axis
      Maintain constant force in the x-direction
      Eliminate rotation error by torque perception
    else if $F_x >= F_{contact}$ & $F_y < F_{contact}$ **then**
      The end of the robot moves along the y-axis
    else if $F_y >= F_{contact}$ & $F_x >= F_{contact}$ **then**
      Rotate for Minimizing the gap with angle α
      Return Done
    End if
  End if
The Gripper releases object
The Manipulator withdraws from the bin

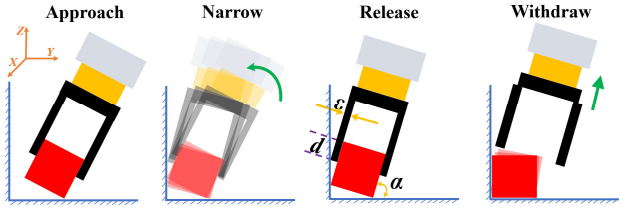

Fig. 3. Illustration of manipulation strategies in Subtask-I.

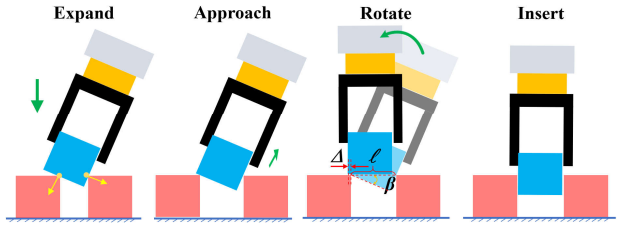

Fig. 4. Illustration of manipulation strategies in Subtask-II.

C. Subtask-II: Packing the Middle Objects

The first eight objects in four corners are compact with each other after Subtask-I. However, potential errors may lead to the middle space being narrower than the size of the object, and it is difficult to insert the object directly. Considering the narrow spaces, we propose a dense packing strategy as Subtask-II to pack the middle objects, as shown in Fig. 4.

At first, the manipulator tilts with an angle β and moves vertically downward until it maintains constant force in the z-direction. In this process, the object in hand will push the objects on both sides to expand the middle space. Then, the manipulator moves towards the constraint direction for tight contact, which can be the surface of the storage bin or another object. Then, the rotation error around the z-axis can be further eliminated by torque perception. After that, the manipulator rotates to horizontal and moves with a distance of Δ, calculated by the object size ℓ and the tilt angle β, as shown in (33). Finally, the object will be inserted by small vibrations once it aligns with the hole because of the constant force applied in the z-direction.

$$\Delta = \ell(1-\cos\beta) \tag{33}$$

D. Subtask-III: Inserting the Last Object

Inserting the object into a limited space can be considered as a peg-in-hole problem. For this problem, there is no general solution to identify the contact state between the peg and the hole. However, we humans can accurately locate the hole, align and insert the peg into the hole, even with eyes closed, as shown in Fig. 5. Inspired by the human assembly, we propose a novel ***Tilt-Then-Move*** method that contains two phases to address this problem, as summarized in Algorithm 2.

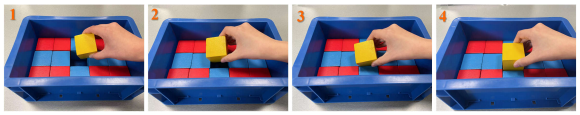

Fig. 5. Peg-in-hole demonstration by human.

When the robot is guided near the desired position, errors in the x and y directions always coexist, meaning that at least one corner of the object is within the hole, as shown in Fig. 1(c). First, we tilt the manipulator in the directions of four corners of the object, respectively. During this process, we compare the position of the end effector in the z-direction. The position in the z-direction will decrease when the object's tip tilts into the hole. In this case, the contact state can be roughly identified at first. During the moving phase, the manipulator tilts towards the hole at first, and then moves in the y-direction to fill the hole and confirms tight contact by force perception, which also contributes to expanding the potential narrow hole through push. Then, the manipulator moves along the x-axis similarly until it confirms tight contact in this direction. Finally, we could insert the object vertically into the hole with the accurate contact state.

Algorithm 2: Strategy for inserting the last object

Input: Six-dimension external force/torque $\boldsymbol{F}_{ext}$, $\boldsymbol{T}_{ext}$, current pose of the end effector $\{\boldsymbol{R}, \boldsymbol{t}\}$
Output: Contact state and Done
Phase 1: Identify the direction of the hole
Maintain Constant force in the z-direction
For *Four directions of the object's corners,* **do**
  Tilt the end effector
  Measure the position of the end effector
Compare the position *in the z-direction:*
$z_i \longleftarrow \{min(z_1, z_2, z_3, z_4, z_{init})\}$
Return The direction of the Phase 2
Phase 2: Align and insert the object
In every force-controlled cycle S_c*:*
  If $F_y < F_{contact}$ **then**
    The end of the robot moves along the y-axis
    Maintain constant force with bin in y-direction
  else if $F_y >= F_{contact}$ & $F_x < F_{contact}$ **then**
    The end effector moves along the x-axis
  else if $F_y >= F_{contact}$ & $F_x >= F_{contact}$ **then**
    Insert the object with small vibrations
    Return Done
The Gripper releases object

VI. EXPERIMENTS

We conduct abundant experiments to evaluate the proposed bin packing pipeline. Concretely, we test the accuracy of our external force estimation algorithm, perform comparison studies with the current packing methods, investigate the performance of our proposed dissipativity-based impedance-force controller, and then validate the generalizability on novel objects with different shapes and sizes.

A. Experimental Setup

We conduct real-world packing experiments on a Franka Emika robot with the Robotiq-140 gripper. The robot is under force control mode, and we send joint torque commands and receive real-time joint states through the ROS topic mechanism. Moreover, the joint torque commands are sent at 1000 Hz, consistent with the computation cycle of our impedance-force controller and proven to be stable. The packing task is arranged as follows: the robot places objects into a storage bin for 5×3 grid configuration tightly. The size of the object is 5×5×5 cm, and the dimension of the bin is 26×16×10 cm.

B. Accuracy of External Force Estimation

Here we perform experiments to quantitatively evaluate the accuracy of our external force estimation algorithm. A standard ATI force sensor is employed under the contact surface to measure the contact force as ground truth, as shown in Fig. 6. The robotic arm performs a series of actions while maintaining contact with the force sensor to sample rich force information. The external force is both estimated by our approach and measured by the ATI sensor during this process.

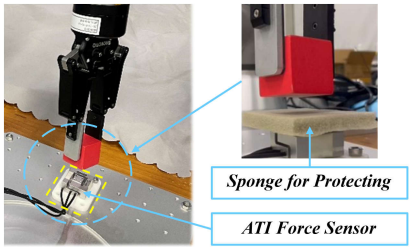

Fig. 6. The standard ATI force sensor is employed under the contact surface to measure the contact force as ground truth for quantitative evaluation.

The experimental results are plotted in Fig. 7. We can observe that the estimated external forces on three axes have minor errors compared to the ground truth, proving the precision of our approach. Moreover, we adopt two metrics to implement quantitative comparison: the mean absolute error (MAE) and the mean absolute percentage error (MAPE). The following results can be obtained from experiments:

1) The MAEs of force are 0.178 N on the *x*-axis, 0.156 N on the *y*-axis, and 0.340 N on the *z*-axis;
2) The MAPEs of force are 5.92% on the *x*-axis, 3.60% on the *y*-axis, and 6.05% on the *z*-axis;
3) Even under long-term dynamic testing, our method can maintain high estimation accuracy within 6% error.

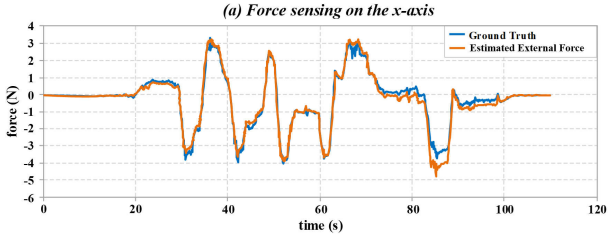

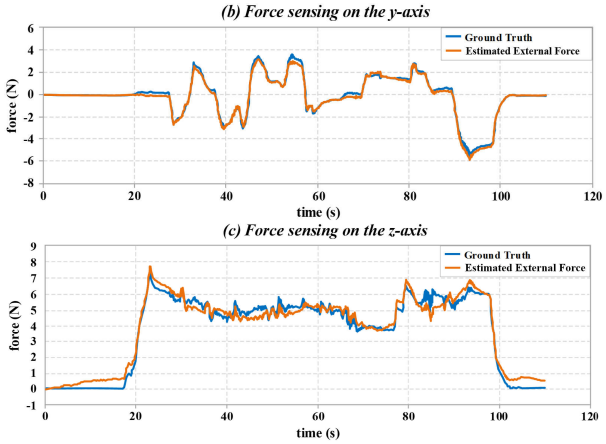

Fig. 7. Force sensing data estimated by our generalized momentum observer and measured by the standard force sensor (ground truth) on three axes.

C. Comparison with Current Packing Methods

Abundant real-world packing experiments are conducted to compare our packing pipeline with current methods. During experiments, the improvements introduced by our method are detailedly evaluated by comparison points in different versions. Concretely, the approach only based on visual input is considered as the baseline, and fifty groups of packing experiments for each version are performed. The successful placement for one object is defined as: the packed object does not exceed 25% of the desired area's volume. The number of successfully packed objects and the consumed time by the whole task are recorded, as shown in Fig. 8.

V1 - (Baseline) Grasping and packing by vision. The baseline solely adopts visual algorithms for grasping and preliminary packing, as described in Section V-A.

V2 - (Baseline + Auxiliary push actions) Based on V1, the additional push actions are applied to eliminate residual gaps and ensure compactness after each placement.

V3 - (Our methodology) Our bin packing pipeline with the visual coarse localization and dense packing strategies using our dissipativity-based impedance-force controller.

V4 - (Controller comparison) The latest passivity-based impedance controller proposed in [32] is adopted to replace our controller in **V3** for comparison.

As shown, V1 exhibits poor accuracy and unstable performance. The maximum number of successfully placed objects is merely 6, indicating that the packing task cannot be completed solely by vision. Meanwhile, the lack of tight packing strategies makes it unable to ensure compactness. In some cases, one improperly packed object may affect subsequent manipulation and even disrupt the whole process. We compute that the visual error $\varepsilon_{visiual}$ is on average 1.2 cm in translation and 0.6 rad in rotation with the method in [3]. Moreover, we can observe that the success rate of V2 is enhanced compared to V1 and the system sometimes can fulfill successful placement for all objects, which proves the effectiveness of auxiliary actions. However, these push-to-place actions are always required after each placement, causing high time expenditure and poor efficiency.

By applying packing strategies, V3 and V4 improve the performance over V1 and V2. However, in our observation, the manipulator with the controller in V4 occasionally collides violently with the storage bin, leading to some unstable situations and even failure, which is also illustrated in Fig. 8 (Left).

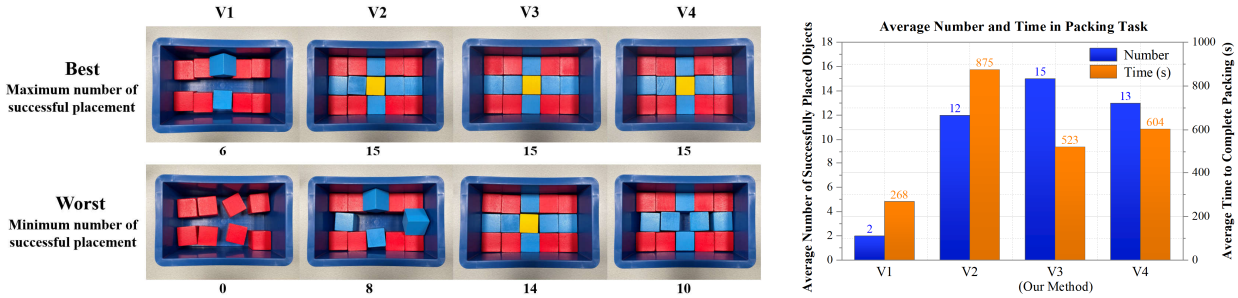

Fig. 8. (Left) The final situation of each version in packing experiments, where every column represents a version. The top row represents the best results, while the bottom row shows the worst results, according to the number of successfully placed objects shown below the figures. (Right) The blue and orange bars represent the average number of successfully placed objects and the average time spent with each version.

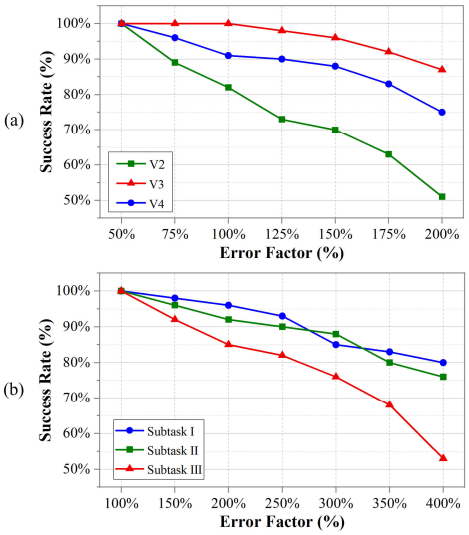

Fig. 9. (a) Packing success rates under varying pose errors with different methods. (b) Packing success rates in each subtask with V3.

In comparison, V3 with our adaptive controller shows more reliable performance in rapid motion tracking and compliant interaction. Compared with V1, our pipeline can accomplish the whole packing task with great improvement in accuracy. Meanwhile, benefiting from the proposed packing strategies, the efficiency of V3 increases by 40% over V2, as shown in Fig. 8 (Right), which is critical for such packing tasks.

D. Evaluation of Contact Force during Interaction

Compliant interaction is desired to ensure robustness and prevent damage to objects in bin packing. Thus, we propose the adaptive impedance-force controller. By adjusting the impedance parameters, the robot can properly react to the established interaction and avoid force overshoots. Meanwhile, the conducted dissipativity analysis helps optimize our controller and ensures system stability. Here we examine the performance of the proposed controller by measuring the contact force during packing and compare it with the latest variable impedance control algorithm [32].

We mount an ATI Mini45 force sensor between the robot TCP and the gripper to measure the contact force by coordinate transformation. The average and maximum contact forces in different subtasks with V3 and V4 are measured and recorded in Table I. Concretely, the average contact force reflects the overall interaction performance, and the soft and stable contact force is desired for this contact-rich task. The maximum contact force is used to evaluate the robotic behavior when encountering obstacles, and excessive forces may indicate potential safety issues. As shown, the interaction process with our adaptive controller turns gentler compared to the latest variable impedance controller, which means fewer impact and safer contact. This proves that our dissipativity-based stability analysis and optimization are quite valuable for the design of control policy. Moreover, it is also worth noting that the advancements introduced by our adaptive controller and packing strategies are not only reflected in safety. These improvements also enhance the accuracy, robustness and efficiency, as reported in Section VI-C. For example, V3 has refined robustness and success rate compared to V4 and effectively improves the packing efficiency over V2.

TABLE I AVERAGE AND MAXIMUM CONTACT FORCES DURING PACKING

Contact force (N)	V3			V4		
	I	II	III	I	II	III
Average force	16.5	21.2	14.6	26.5	32.2	20.9
Maximum force	26.7	32.1	22.4	38.6	53.4	30.2

E. Performance under Varying Pose Errors

We further investigate the robustness of our packing system under varying initial errors, which denote the deviation between the preliminary poses guided by vision and the desired packing poses. We adjust the initial error ε_{init} with an error factor and initialize the manipulator near the desired packing pose with the predefined error:

$$\varepsilon_{init} = error\ factor \times \varepsilon_{visual} \tag{34}$$

When the error factor is 100%, the initial error is equal to the visual error ε_{visual}, which is 1.2 cm in translation and 0.6 rad in rotation, as measured in VI-C. A total of twenty groups of packing experiments under different error factors are performed for V2, V3 and V4. The success rate, which is denoted by the percentage of objects successfully placed for each version is recorded. Furthermore, the performance of our pipeline V3 in each subtask is also assessed under a wider margin of initial errors. These results are plotted in Fig. 9.

As shown in Fig. 9(a), as the error factor increases, the success rates of V2 decrease rapidly, especially when the error factor is larger than 100%. In comparison, V3 can maintain an 87% success rate even when the error factor comes to 200%, which means high requirements for robustness. Meanwhile, the comparison between V3 and V4 further indicates the proposed adaptive impedance-force controller can improve the interaction performance and enhance the packing accuracy. Besides, as presented in Fig. 9(b), the pose error has a small impact on Subtask-I and Subtask-II but greatly influences Subtask-III. We speculate that the pose error has a considerable effect on the contact state identification, making it difficult to locate the hole and even infer the wrong direction. Moreo-

ver, the success rate of each subtask decreases rapidly when the error factor is larger than 300%, indicating excessive pose errors may lead to instability of the packing system.

F. Packing Multi-layer and Novel Objects

We perform our pipeline on a multi-layer packing task, as shown in Fig. 10(a). A total of twenty groups of experiments are conducted, and only one group fails due to the excessive friction with the underlying objects. The results indicate that the manipulation of placing the second layer beyond the first plane is effective by running the same methods.

Moreover, to validate the applicability of our approach to cylindrical and different-size objects, twenty groups of packing experiments are performed, as shown in Fig. 10(b). The results prove that our pipeline is not restricted by shapes and sizes, and can be directly applied with simple fine-tuning. The average success rate of object tight placement is 86%.

(a) (b)

Fig. 10. Results for packing multi-layer and novel objects.

VII. Conclusion

This paper presents an efficient and robust packing pipeline. The introduced generalized momentum observer avoids the influence of joint acceleration noises and achieves high-precision external force monitoring. Benefiting from the developed adaptive impedance-force controller, the robot can achieve fine motion tracking and properly react to the established interaction to enhance robustness. Then, the conducted dissipative analysis reveals the stability mechanism of the system and optimizes the controller with an augmented virtual energy supply function. Moreover, the proposed packing strategies in three subtasks eliminate the need for subsequent auxiliary actions and effectively improve the packing efficiency. Comprehensive experiments prove the proposed packing pipeline with our dissipativity-based adaptive controller and packing strategies outperforms the existing methods. These performance gains prove our work is fruitful for efficient and robust bin packing. Future work will explore universal packing methods for more different-shape objects.

References

[1] A. Lodi, M. Monaci, and E. Pietrobuoni, "Partial enumeration algorithms for Two-Dimensional Bin Packing Problem with guillotine constraints," *Discrete Applied Mathematics*, vol. 217, pp. 40–47, Jan. 2017.

[2] B. Mahvash, A. Awasthi, and S. Chauhan, "A column generation-based heuristic for the three-dimensional bin packing problem with rotation," *Journal of the Operational Research Society*, vol. 69, no. 1, pp. 78–90, Jan. 2018.

[3] F. Wang and K. Hauser, "Dense Robotic Packing of Irregular and Novel 3D Objects," *IEEE Trans. Robot.*, vol. 38, no. 2, pp. 1160–1173, Apr. 2022.

[4] M. Schwarz *et al.*, "Fast Object Learning and Dual-arm Coordination for Cluttered Stowing, Picking, and Packing," in *2018 IEEE International Conference on Robotics and Automation (ICRA)*, Brisbane, QLD: IEEE, May 2018, pp. 3347–3354.

[5] D. Morrison *et al.*, "Cartman: The Low-Cost Cartesian Manipulator that Won the Amazon Robotics Challenge," in *2018 IEEE International Conference on Robotics and Automation (ICRA)*, Brisbane, QLD: IEEE, May 2018, pp. 7757–7764.

[6] M. Agarwal, S. Biswas, C. Sarkar, S. Paul, and H. S. Paul, "Jampacker: An Efficient and Reliable Robotic Bin Packing System for Cuboid Objects," *IEEE Robot. Autom. Lett.*, vol. 6, no. 2, pp. 319–326, Apr. 2021.

[7] R. Shome *et al.*, "Towards Robust Product Packing with a Minimalistic End-Effector," in *2019 International Conference on Robotics and Automation (ICRA)*, Montreal, QC, Canada: IEEE, May 2019, pp. 9007–9013.

[8] A. Cosgun, T. Hermans, V. Emeli, and M. Stilman, "Push planning for object placement on cluttered table surfaces," in *2011 IEEE/RSJ International Conference on Intelligent Robots and Systems*, San Francisco, CA: IEEE, Sep. 2011, pp. 4627–4632.

[9] J. E. King, J. A. Haustein, S. S. Srinivasa, and T. Asfour, "Nonprehensile whole arm rearrangement planning on physics manifolds," in *2015 IEEE International Conference on Robotics and Automation (ICRA)*, Seattle, WA, USA: IEEE, May 2015, pp. 2508–2515.

[10] T. Gabriel, G. Perboli, and R. Tadei, "Recent Advances in Multi-dimensional Packing Problems," in *New Technologies - Trends, Innovations and Research*, C. Volosencu, Ed., InTech, 2012.

[11] S. Hayashi *et al.*, "Automation technologies for strawberry harvesting and packing operations in Japan1," *JBR*, vol. 4, no. 1, pp. 19–27, Apr. 2014.

[12] A. Zeng *et al.*, "Robotic Pick-and-Place of Novel Objects in Clutter with Multi-Affordance Grasping and Cross-Domain Image Matching," in *2018 IEEE International Conference on Robotics and Automation (ICRA)*, Brisbane, QLD: IEEE, May 2018, pp. 3750–3757.

[13] D. Hutchison *et al.*, "Two Natural Heuristics for 3D Packing with Practical Loading Constraints," in *PRICAI 2010: Trends in Artificial Intelligence*, vol. 6230, B.-T. Zhang et al., in Lecture Notes in Computer Science, vol. 6230. , Berlin, Heidelberg: Springer Berlin Heidelberg, 2010, pp. 256–267.

[14] J. Egeblad, "Placement of two-and three-dimensional irregular shapes for inertia moment and balance," *Int Trans Operational Res*, vol. 16, no. 6, pp. 789–807, Nov. 2009.

[15] E. Spyrakos-Papastavridis and J. S. Dai, "Minimally Model-Based Trajectory Tracking and Variable Impedance Control of Flexible-Joint Robots," *IEEE Trans. Ind. Electron.*, vol. 68, no. 7, pp. 6031–6041, Jul. 2021.

[16] W. He and Y. Dong, "Adaptive Fuzzy Neural Network Control for a Constrained Robot Using Impedance Learning," *IEEE Trans. Neural Netw. Learning Syst.*, vol. 29, no. 4, pp. 1174–1186, Apr. 2018.

[17] P. Zou, Q. Zhu, J. Wu, and R. Xiong, "Learning-based Optimization Algorithms Combining Force Control Strategies for Peg-in-Hole Assembly," in *2020 IEEE/RSJ International Conference on Intelligent Robots and Systems (IROS)*, Las Vegas, NV, USA: IEEE, Oct. 2020, pp. 7403–7410.

[18] Z. Du, W. Wang, Z. Yan, W. Dong, and W. Wang, "Variable Admittance Control Based on Fuzzy Reinforcement Learning for Minimally Invasive Surgery Manipulator," *Sensors*, vol. 17, no. 4, p. 844, Apr. 2017.

[19] M. Bogdanovic, M. Khadiv, and L. Righetti, "Learning Variable Impedance Control for Contact Sensitive Tasks," *IEEE Robot. Autom. Lett.*, vol. 5, no. 4, pp. 6129–6136, Oct. 2020.

[20] C. Li, Z. Zhang, G. Xia, X. Xie, and Q. Zhu, "Efficient Force Control Learning System for Industrial Robots Based on Variable Impedance Control," *Sensors*, vol. 18, no. 8, p. 2539, Aug. 2018.

[21] Y. Pei, G. Obinata, Y. Kim, and J. Lee, "Adaptive impedance control with variable viscosity for motion and force tracking system," in *2015 International Symposium on Micro-NanoMechatronics and Human Science (MHS)*, Nagoya, Japan: IEEE, Nov. 2015, pp. 1–5.

[22] J. Duan, Y. Gan, M. Chen, and X. Dai, "Adaptive variable impedance control for dynamic contact force tracking in uncertain environment," *Robotics and Autonomous Systems*, vol. 102, pp. 54–65, Apr. 2018.

[23] X. Zhang, L. Sun, Z. Kuang, and M. Tomizuka, "Learning Variable Impedance Control via Inverse Reinforcement Learning for Force-Related Tasks," *IEEE Robot. Autom. Lett.*, vol. 6, no. 2, pp. 2225–2232, Apr. 2021.

[24] H. Cao, X. Chen, Y. He, and X. Zhao, "Dynamic Adaptive Hybrid Impedance Control for Dynamic Contact Force Tracking in Uncertain Environments," *IEEE Access*, vol. 7, pp. 83162–83174, 2019.

[25] H. Cao, Y. He, X. Chen, and X. Zhao, "Smooth adaptive hybrid impedance control for robotic contact force tracking in dynamic environments," *IR*, vol. 47, no. 2, pp. 231–242, Feb. 2020.

[26] A. Naceri, T. Schumacher, Q. Li, S. Calinon, and H. Ritter, "Learning Optimal Impedance Control During Complex 3D Arm Movements," *IEEE Robot. Autom. Lett.*, vol. 6, no. 2, pp. 1248–1255, Apr. 2021.

[27] A. Colomé et al., "Robot Compliant Control," in *Reinforcement Learning of Bimanual Robot Skills*, vol. 134, in Springer Tracts in Advanced Robotics, vol. 134. , Cham: Springer International Publishing, 2020, pp. 53–72.

[28] J. Ding, C. Wang, and C. Lu, "Transferable Trial-Minimizing Progressive Peg-in-hole Model," in *2019 IEEE/RSJ International Conference on Intelligent Robots and Systems (IROS)*, Macau, China: IEEE, Nov. 2019, pp. 5862–5868.

[29] S. Liu, D.-P. Xing, Y.-F. Li, J. Zhang, and D. Xu, "Robust Insertion Control for Precision Assembly With Passive Compliance Combining Vision and Force Information," *IEEE/ASME Trans. Mechatron.*, vol. 24, no. 5, pp. 1974–1985, Oct. 2019.

[30] M. Arcak, C. Meissen, and A. Packard, *Networks of Dissipative Systems*. in SpringerBriefs in Electrical and Computer Engineering. Cham: Springer International Publishing, 2016.

[31] M. Sundermeyer, et al., "Implicit 3D Orientation Learning for 6D Object Detection from RGB Images," in *Computer Vision – ECCV 2018*, vol. 11210, V. Ferrari, M. Hebert, C. Sminchisescu, and Y. Weiss, Eds., in Lecture Notes in Computer Science, vol. 11210. , Cham: Springer International Publishing, 2018, pp. 712–729.

[32] F. Voigt, et al., "I ^{2} mpedance - A Passivity Based Integrative Impedance Controller for Precise and Compliant Manipulation and Interaction," in *2023 IEEE/RSJ International Conference on Intelligent Robots and Systems (IROS)*, Detroit, MI, USA: IEEE, Oct. 2023, pp. 4472–4479.